ACS OMEGA

Open Access

http://pubs.acs.org/journal/acsodf

Article

6-Aza-2-Thiothymine-Capped Gold Nanoclusters as Robust Antimicrobial Nanoagents for Eradicating Multidrug-Resistant *Escherichia coli* Infection

Hui-Qiong Jiang,[⊥] Lin-Yan Lu,[⊥] Zhi-Min Weng, Kai-Yuan Huang, Yu Yang, Hao-Hua Deng, Ying-Ying Xu,* Wei Chen,* and Quan-Quan Zhuang*

Cite This: *ACS Omega* 2023, 8, 47123−47133

Read Online

ACCESS | Metrics & More | Article Recommendations | Supporting Information

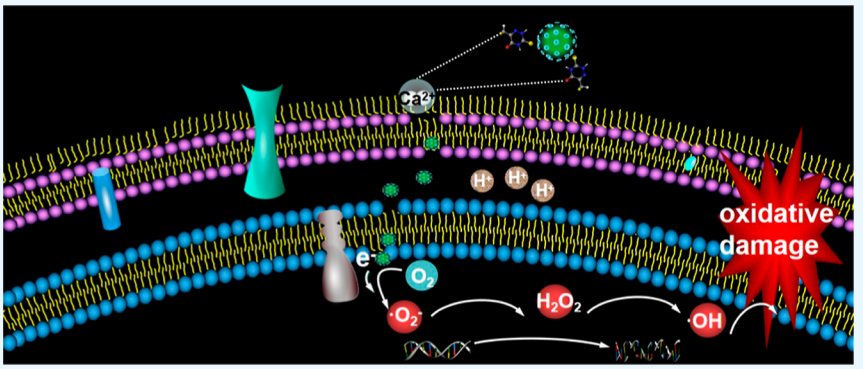

ABSTRACT: Multidrug-resistant bacterial infections, especially those caused by multidrug-resistant *Escherichia coli* (*E. coli*) bacteria, are an ever-growing threat because of the shrinking arsenal of efficacious antibiotics. Therefore, it is urgently needed to develop a kind of novel, long-term antibacterial agent effectively overcome resistant bacteria. Herein, we present a novel designed antibacterial agent—6-Aza-2-thiothymine-capped gold nanoclusters (ATT-AuNCs), which show excellent antibacterial activity against multidrug-resistant *E. coli* bacteria. The prepared AuNCs could permeabilize into the bacterial cell membrane via binding with a bivalent cation (e.g., Ca^{2+}), followed by the generation of reactive oxygen species (e.g., $^{\bullet}OH$ and $^{\bullet}O^{2-}$), ultimately resulting in protein leakage from compromised cell membranes, inducing DNA damage and upregulating pro-oxidative genes intracellular. The AuNCs also speed up the wound healing process without noticeable hemolytic activity or cytotoxicity to erythrocytes and mammalian tissue. Altogether, the results indicate the great promise of ATT-AuNCs for treating multidrug-resistant *E. coli* bacterial infection.

1. INTRODUCTION

In the 21st century, antimicrobial resistance (AMR) is a global health crisis with the highest burden in resource-limited settings. Currently, it has been estimated that the annual death rate caused by AMR would be over seven million and is hypothesized to approach nearly ten million deaths in 2050.[1] Among the six leading pathogens, multidrug-resistant *Escherichia coli* (MDR *E. coli*) tops the list in causing a wide range of deaths due to their high prevalence. The most important of the inherent weakness of antibiotics is the development of resistance caused by MDR *E. coli*. The frequent tools of the bacteria against a variety of antimicrobials are efflux pumps, production of β-lactamase, or mutations of bacterial membrane transporters.[2,3] Therefore, it is highly desirable to exploit novel and efficient theranostic approaches to kill MDR *E. coli* bacteria.

Antimicrobial peptides (AMPs), which are found in multiple niches in nature and generally consist of 10−40 amino acid residues, have excellent antibacterial activities.[4] Yang et al. reported a kind of AMP with cationic and amphiphilic structures, which can disintegrate Gram-negative bacteria via inserting into their cell surfaces.[5] Compared with conventional antibiotics, one of the strengths of AMPs is their low propensity for resistance development; however, AMPs show high cost and hemolysis in vivo, and the poor antibacterial activity and salt instability also limit their clinical implementation.[6] In fact, a relatively new field of nanotechnology has

Received: September 17, 2023
Revised: November 14, 2023
Accepted: November 20, 2023
Published: November 28, 2023

opened the new possibilities of designing effective formulations for fighting antibiotic resistance.[7]

Metal-based antibacterial therapeutics, such as silver nanoparticles,[8] ZnO nanoparticles,[9] and iron oxide nanoparticles,[10,11] have attracted growing interest due to their efficiency of antimicrobial properties, no resistance development, and convenient for transporting. In addition, photocatalytic antimicrobial TiO_2 nanoparticle is also explored to treat MDR bacteria-caused infections.[12] However, the antimicrobial activity of the photocatalytic substances is severely limited in the absence of light. The utilization of nanomaterials mentioned above is also extremely limited in the field of medicine due to complex processing, potential cytotoxicity, and environmental pollution.[13]

Metal nanoclusters with intriguing molecular-like structure have received extensive attention due to their remarkable photoelectrical properties.[14] Among various metal nanoclusters, gold nanoclusters with unique chemical and physical properties have been extensively researched to be emerging nanoantibiotics for fighting bacterial infections.[15] Quaternary ammonium (QA) capped AuNCs and mercaptobenzoic acid-functionalized AuNCs had been reported as novel agents targeting Gram-positive bacterial strains.[16,17] However, there are only a few reports on the activity of AuNCs against Gram-negative bacterium. Wang et al. demonstrated mercaptopyrimidine conjugated Au NCs could act as potent nanoantibiotics targeting MDR *E. coli*.[18] Nevertheless, bactericidal activity from the assistance of H_2O_2 would be expected to arise as disadvantages to healthy tissue. MUTAB-AuNCs and Cys-AuNCs had also been proved to exhibit efficient antibacterial activity against *E. coli* bacteria.[19,20] Unfortunately, these AuNCs have not been evaluated for their effects on MDR *E. coli*. At present, designing and synthesizing unique features of AuNCs that can overcome MDR *E. coli* bacteria with high efficacy remain a great challenge.

In this work, we reported a kind of gold nanocluster (ATT-AuNCs), which could be used as efficient antimicrobial nanoagents for eliminating MDR *E. coli* bacteria. After the confirmation of bactericidal activity, we systematically study the distinctive antimicrobial mechanism of ATT-AuNCs and their effects on an in vivo infection model caused by MDR *E. coli*. In addition, the AuNCs exhibit negligible hemolysis or cytotoxicity for mammal cells and tissues. We expect that our results will offer valuable information for future development of AuNCs toward MDR *E. coli*.

2. EXPERIMENTAL SECTION

2.1. Synthesis of ATT-AuNCs. Briefly, the mixture was prepared by dissolution of 115 mg of ATT in 10 mL of NaOH (0.2 M), followed by continuous stirring in 10 mL of 10 mg/mL $HAuCl_4$ solution for 1 h at 25 °C in the dark. The prepared ATT-AuNCs were dialyzed against 500 mL of deionized water for 24 h using a dialysis membrane with a molecular weight cutoff of 3500.[21]

2.2. Antibacterial Activity of ATT-AuNCs. MDR *E. coli* strains were cultured in Luria−Bertani (LB) medium at 35 °C for 24 h. Cell growth was followed by measuring the McFarland scale at 0.5 index (1.5×10^8 CFU/mL).[22] Next, ATT-AuNCs were serially diluted from 32.0 to 2.0 μg/mL and then 10 μL of MRSA cells and 170 μL of LB broth were added into each well. Control group contained no AuNCs. The plates were incubated for 18 h at 35 °C. The mixture was diluted to 10^5-fold with 0.9% NS. Then, one hundred microliters of each sample was spotted onto a blood agar plate, followed by incubation at 35 °C for 16 h to count the surviving bacterial colonies by using ImageJ software. All treatments were performed on three separate occasions. The bacterial viability rate (VR) was calculated as follows

$$\text{VR}\ (\%) = (\text{the number of experimental bacterial cells}) / (\text{the number of control bacterial cells})$$

2.3. Inhibitory Bacterial Growth Curve Assay. Serial concentrations of ATT-AuNCs (2, 4, 8, 16, and 32 μg/mL) were mixed with the fresh bacterial culture (10 μL, 0.5 McFarland scale) in 170 μL of LB broth and were incubated at 35 °C. Ultrapure water was set as control. The values of bacterial optical density (OD_{600}) were detected every 2 h to monitor the bacterial growth using an Infinite M200 spectrophotometer (Tecan, Switzerland).[23]

2.4. Scanning Electron Microscopy and Transmission Electron Microscopy of Bacterial Samples. The bacterial solution (2.0 mL) was incubated with ATT-AuNCs solution (32 μg/mL) for 20 h, and then, the solution was centrifuged at 13,000 rpm for 5 min. Phosphate buffer (pH 7.4, 1.0 mL) containing 2.5% glutaraldehyde was added to the samples and incubated overnight at 4 °C for fixation. We sequentially used water−ethanol and ethanol−Freon solutions (20, 50, 80, and 100% concentration for each solvent) to wash and dehydrate the samples. Finally, samples were air-dried and gold-coated before examining using TecnaiG2F20 scanning electron microscopy (SEM). The bacteria were further processed for transmission electron microscopy (TEM) observation; after propylene oxide treatment, the stained cells were finally embedded in Epon. Ultrathin sections (50 nm) were obtained using an ultramicrotome (EM UC7, LEICA, Germany) and poststained with uranyl acetate and lead citrate for 15 min. The sections were observed for TEM at 100 kV (JEM-1200EX, JEOL, Japan).[24]

2.5. Relative Gene Expression. RNA extraction from ATT-AuNC-treated bacteria was carried out using a RNeasy mini kit (R402-01-AB, Vazyme, China) according to the manufacturer's protocol.[25] A NanoDrop 2000 spectrophotometer (Thermo Scientific, USA) was used to quantify the concentrations of RNA and then RNA was reverse transcribed into cDNA using a HiScript III first Strand cDNA Synthesis Kit (R312-01, Vazyme, China). The quantitative PCR was conducted in a CFX96TM Real-Time PCR Detection System (Bio-Rad, USA). The PCRs were performed in a 20 μL volume containing 10 μL of ChamQ Universal SYBR qPCR Master Mix (Vazyme, Q711−02, China), 0.4 μL of forward and reverse primers (10 μM), 5 μL of template cDNA, and 4.2 μL of ddH_2O. *gyrB* was used as an internal control. The design of primer sequences of each gene were performed according to the reported assay.[26]

2.6. Hemolysis Effects of ATT-AuNCs. A previously reported hemolysis assay was used to further evaluate blood compatibility.[27] 0.2 mL of blood suspension was diluted with 0.9% NS and incubated at various ATT-AuNC concentrations (0.8 mL, 0, 8, 16, 32 64, 128, and 256 μg/mL). Water and 0.1% Triton-X were chosen as positive controls. After 2 h of incubation at room temperature, the mixture was centrifuged at 1000 rpm for 10 min. We recorded the absorbance of the supernatant at 540 nm using an Infinite M200 spectrophotometer (Tecan, Switzerland) to evaluate the blood compatibility of ATT-AuNCs.

https://doi.org/10.1021/acsomega.3c07114
ACS Omega 2023, 8, 47123−47133

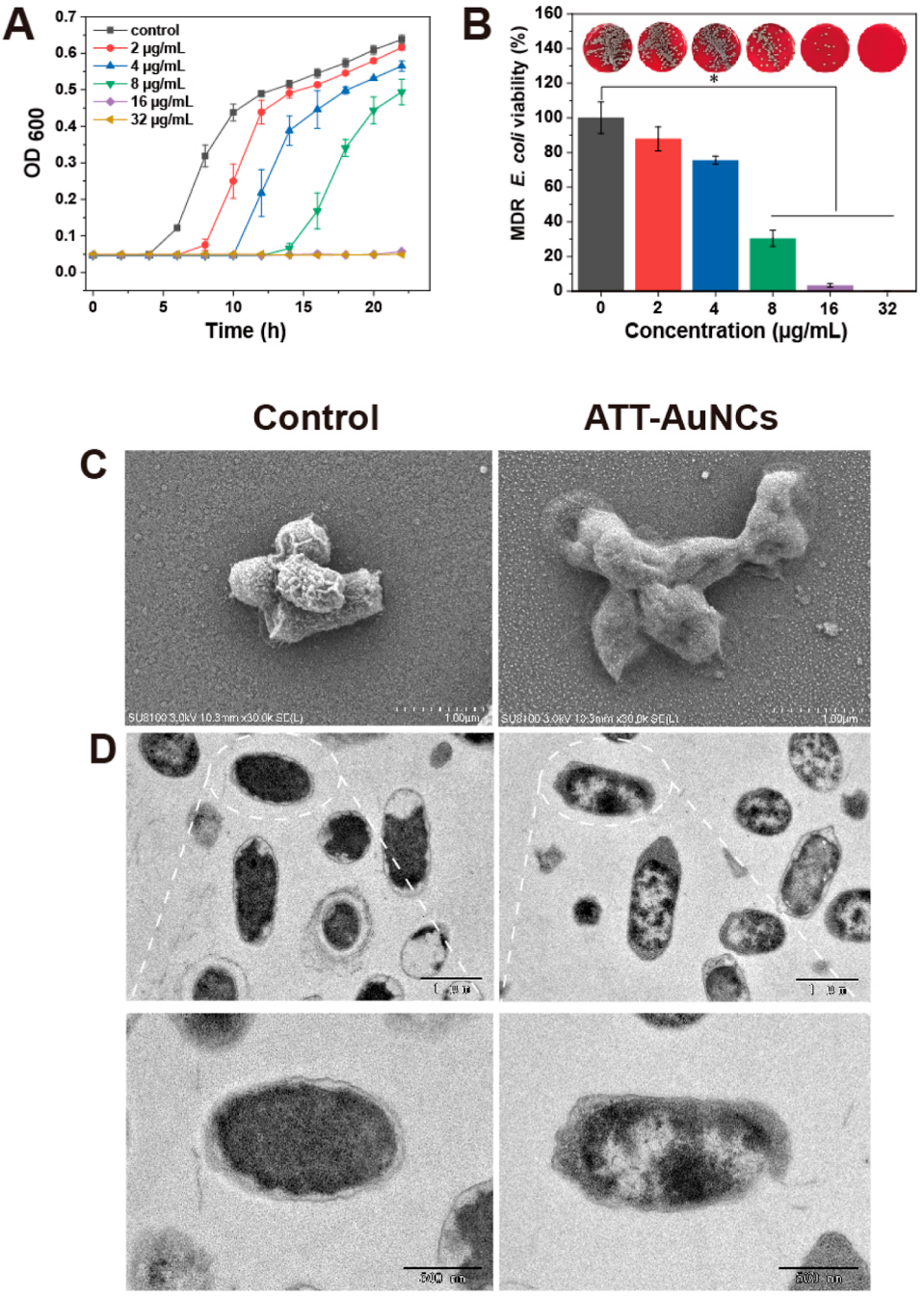

Figure 1. (A) Time-dependent bacterial OD $_{600}$ of MDR *E. coli* treated with ATT-AuNCs (0−32 μg/mL). (B) Survival rates of MDR *E. coli* incubated at various ATT-AuNCs concentrations (0, 2, 4, 8, 16, and 32 μg/mL). Insets are the corresponding digital photographs of the colony-forming units of MDR *E. coli*. SEM (C) and TEM (D) images of MDR *E. coli* treated with water or ATT-AuNCs at 35 °C for 20 h.

2.7. Mouse Injury Model and Wound Healing. All animal procedures were in accord with the guidelines of the Institutional Animal Care and Use Committee of Quanzhou Medical College (2022001). The injury model was built to investigate the antibacterial activity of the ATT-AuNCs in vivo. Two groups of 6 Sprague−Dawley (SD) rats with a *ca.* 2.25 cm^2 wound were divided into water and ATT-AuNCs groups. Then, 200 μL of MDR *E. coli* suspension (1.5×10^8 CFU/mL) was placed on the wound site to make an infected wound model. Photos were taken of the wound of rats from both groups, and solution treatment was changed at 24 h interval. After sacrifice at 12 days, the wound tissues and main organs of all rats were collected for further analysis.

2.8. Immunohistochemistry and Immunofluorescence Analysis. The harvested organs and wound tissues were fixed in 4% paraformaldehyde. Subsequently, the samples were embedded in paraffin, cut into slices and stained with histopathological hematoxylin and eosin (H&E) or Masson's trichrome (MT). For immunohistochemical staining, tumor necrosis factor-α (TNF-α) and interleukin-10 (IL-10) were adopted to evaluate the degree of inflammation. For immunofluorescence staining, CD68 was also assessed to reflect the regulation of macrophage cells. ImageJ software was used to quantify the histochemical analysis results.

https://doi.org/10.1021/acsomega.3c07114
ACS Omega 2023, 8, 47123−47133

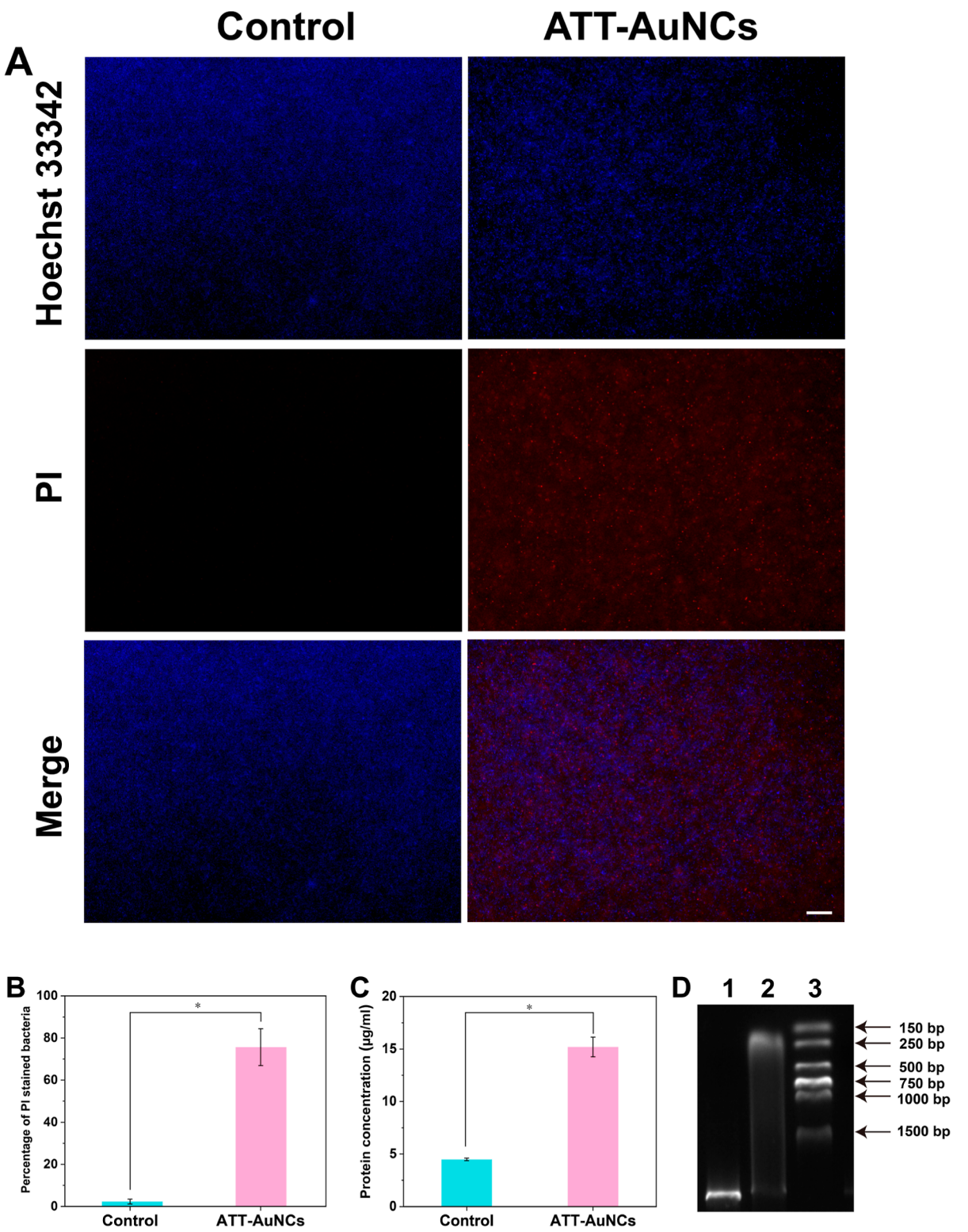

Figure 2. (A) Fluorescence images of MDR *E. coli* after incubation with water or ATT-AuNCs for 20 h. PI staining represents dead bacterial cells (red color). Hoechst 33342 staining represents both dead and living cells (blue color). Scale bar: 25 μm. (B) Percentage of the damaged bacterial membrane stained using PI. (C) Protein leakage from MDR *E. coli* suspensions treated with ATT-AuNCs. (D) Genomic DNA degradation of MDR *E. coli* after treatment with ATT-AuNCs. Lanes 1−3 correspond to water, ATT-AuNCs treatments, and marker, respectively.

3. RESULTS AND DISCUSSION

3.1. Characterization and the Antimicrobial Activities of ATT-AuNCs. ATT-AuNCs were synthesized and characterized according the previous report.[28] Figure S1A displays the typical absorption spectra of the as-prepared yellow colored ATT-AuNCs, which showed two absorption bands centered on 387 and 475 nm (inset of Figure S1A). Furthermore, the Au SPR absorption peak located at 520 nm cannot be found. As displayed in the inset of Figure S1B, very weak green fluorescence emitted by ATT-AuNCs when

https://doi.org/10.1021/acsomega.3c07114
ACS Omega 2023, 8, 47123−47133

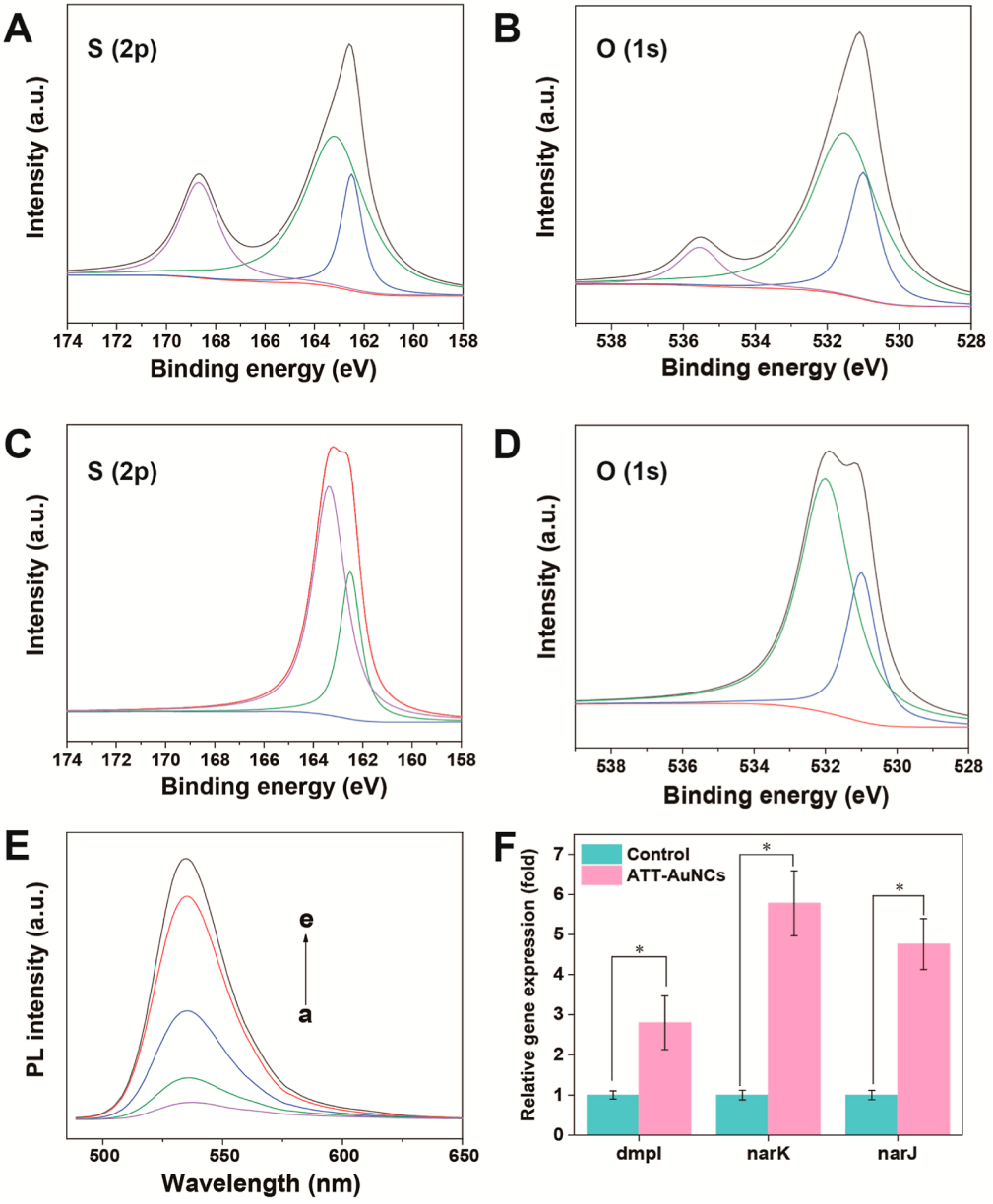

Figure 3. XP spectrum of S (2p) (A,C) and O (1s) (B,D) in ATT-AuNCs before and after interaction with calcium chloride. (E) Increasing of ATT-AuNCs emission by different concentrations of calcium chloride (a-e: 0, 0.5, 1, 2, and 4 mM). (F) Relative gene expression of MDR *E. coli* after treatment with water and ATT-AuNCs for 20 h, respectively.

irradiated with UV light. Two maximal excitation wavelengths were located at 390 and 450 nm, and the photoemission maxima were observed at 539 nm (Figure S1B). The TEM and HRTEM images of ATT-AuNCs are shown in Figure S1C. Lattice fringes are observed with an inner-plane spacing of 0.24 nm, indicating the (111) planes of gold.[29] Meanwhile, ATT-AuNCs measured from 100 individual particles exhibits an average size of 1.77 ± 0.4 nm (Figure S1D). The survey spectrum in Figure S1E confirmed the presence of O(1s), C(1s), N(1s), Au(4f), and S(2p) in ATT-AuNCs, indicating that ATT capped on the gold core. High resolution 4f photoelectron spectra measured from Au (Figure S1F) shows that the binding energy of Au $4f_{7/2}$ is 84.6 eV, which is close to 84.4 eV (Au^{+}), revealing the coexistence of Au(0) and Au(I).[30] The best-fit model for the data illustrated that the percentage of Au(I) in the ATT-AuNCs was approximately 45.4%.

The growth curves of MDR *E. coli* displayed that the addition of ATT-AuNCs obviously inhibited the growth of MDR *E. coli* and the inhibitory effect increased as the ATT-AuNCs concentration increased. The minimal inhibit concentration (MIC) value of ATT-AuNCs toward MDR *E. coli* was defined as 16 μg/mL (Figure 1A). To explore the antibacterial activity, a microbial colony counting method was carried out. The mixture of bacterial solution and ATT-AuNCs were plated and incubated at 35 °C for 20 h. A clear reduction in bacterial colonies was observed on blood agar plates containing a high concentration of ATT-AuNCs (inset of Figure 2A). Furthermore, the concentration dependence of antibacterial activities on AuNC-based materials was studied. ATT-AuNCs solutions at various concentrations (2, 4, 8, 16, and 32 μg/mL) were incubated with MDR *E. coli* cells. As displayed in Figure 2A, the VR of MDR *E. coli* decreased from 87.9% at the ATT-AuNCs concentration of 2 μg/mL to 0 at 32 μg/mL. These

https://doi.org/10.1021/acsomega.3c07114
ACS Omega 2023, 8, 47123−47133

Scheme 1. Illustration of the Synthesis of ATT-AuNCs and Their Possible Mechanism of Bactericidal Effects[a]

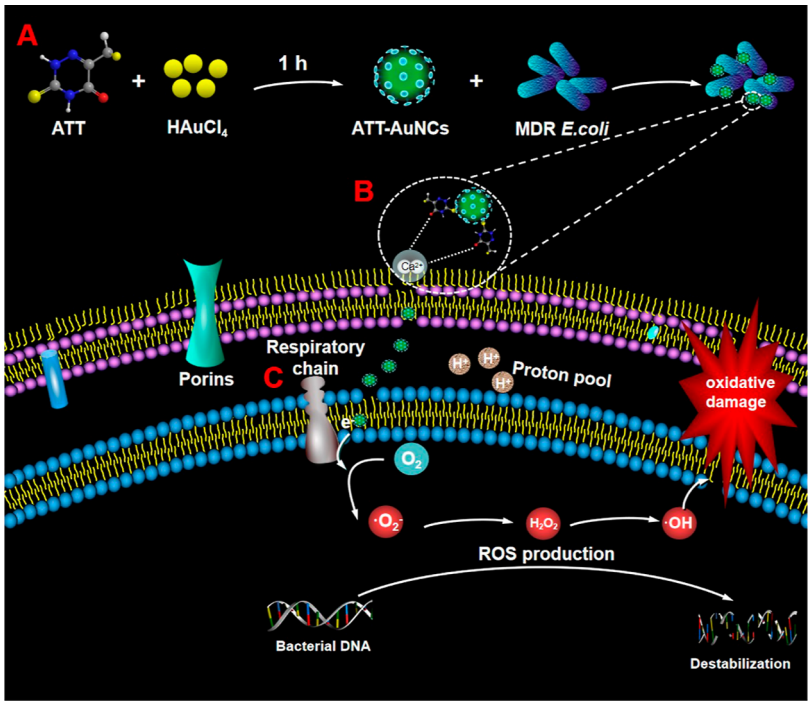

[a](A) ATT-AuNCs are fabricated by mixing 6-Aza-2-thiothymine and chloroauric acid in one step. (B) ATT-AuNCs show electrostatic attraction to bacteria via binding with Ca^{2+} on the bacterial cell wall. (C) ATT-AuNCs on the cell wall may disturb electronic flow through the respiratory chain. Accumulated electrons could be transferred to O_2 to form O_2^-, H_2O_2, and $^{\bullet}OH$, resulting in membrane oxidative damage, protein leakage, and DNA destabilization in bacteria.

results exhibited the strong antibacterial activity of ATT-AuNCs against MDR *E. coli*. To acquire further evidence for better understanding of the antibacterial behaviors, SEM and TEM were employed to visualize a bacterial morphology.[31,32] The untreated bacteria showed smooth and intact cell membrane structures (left of Figure 1C and D). In contrast, the morphologies of MDR *E. coli* were severely collapsed, shrunken, and fused together after being exposed to ATT-AuNCs (right of Figure 1C and D).

The live/dead microbial viability assays of MDR *E. coli* after incubation with water and ATT-AuNCs for 20 h are shown in Figure 2A,B. Almost water-treated bacteria fluoresced strong blue, whereas ATT-AuNC-treated bacteria fluoresced blue as well as red, revealing partial bacteria-killing efficacy of ATT-AuNCs was achieved.[33] In addition, the corresponding images translated into digital information based on ImageJ software indicated that MDR *E. coli* exhibited 2.3% bacterial membrane damage in the control group, whereas in the ATT-AuNCs group, the cells showed 75.7% bacterial cell death (Figure 2C). Protein leakage analysis in MDR *E. coli* cells was further performed by Bradford assay after 20 h treatment to investigate the bactericidal mechanism of ATT-AuNCs.[34] As displayed in Figure 2D, the concentration of leaking protein in the ATT-AuNCs group was higher than that in the water-treated group (15.2 vs 4.5 μg/mL). Therefore, the damage to cell integrity was also considered to be the antimicrobial mechanism of ATT-AuNCs. Additionally, DNA degradation triggered by ATT-AuNCs was assessed. As seen from 1% agarose gel electrophoresis (Figure 2E), the control group showed that genomic DNA remained stable. By contrast, DNA degradation was obviously triggered following treatment with ATT-AuNCs.

3.2. Mechanism of Antibacterial Activity of ATT-AuNCs. In bacteria, many of the cellular processes involved in the cell cycle and division are mediated by bivalent cations (e.g., Ca^{2+}). In addition to cell wall, Ca^{2+} also plays a vital role in structurally stabilizing the integrity of the outer lipopolysaccharide layer.[35] Fluoroquinolones or other antibacterial agent such as daptomycin have been claimed to permeabilize the outer membrane and to exert this function by chelating outer membrane-bound divalent cations.[36] However, a similar effect based on AuNCs induced by bivalent cation has seldom been reported. Herein, the recognition mechanism of ATT-AuNCs toward bivalent cation (e.g., Ca^{2+}) was first investigated. As displayed in Figure 3E, with increasing concentrations of calcium chloride, the fluorescence intensity of ATT-AuNCs gradually increased. In addition, from the XPS characterization results described in Figure 3A−D, after the reaction of Ca^{2+} with ATT-AuNCs, peaks belonging to the S bond and the O bond on the surface of AuNCs disappeared at 168.9 and 535.5 eV, respectively. These indicated that Ca^{2+} on the surface of the MRD *E. coli* could bond with the sulfur- and oxygen- containing functional group of ATT-AuNCs.[37] The electron spin resonance is a recognized technique to detect free radicals. Here, the detection of the hydroxyl radical and superoxide was carried out using 5,5-dimethyl-1-pyrroline *N*-oxide as a spin trap. As shown in Figure S2, when ATT-AuNCs were added, the hydroxyl radical ($^{\bullet}OH$) and superoxide anion radical ($^{\bullet}O^{2-}$) signal were observed. These results indicate that ROS generated by ATT-AuNCs significantly enhances antibacterial activity toward MDR *E. coli*. Furthermore, Three oxidative genes (eg, dmpI, narJ, and narK) of responsible metabolic enzymes were selected for the measurement of ATT-AuNC-treated effect

https://doi.org/10.1021/acsomega.3c07114
ACS Omega 2023, 8, 47123−47133

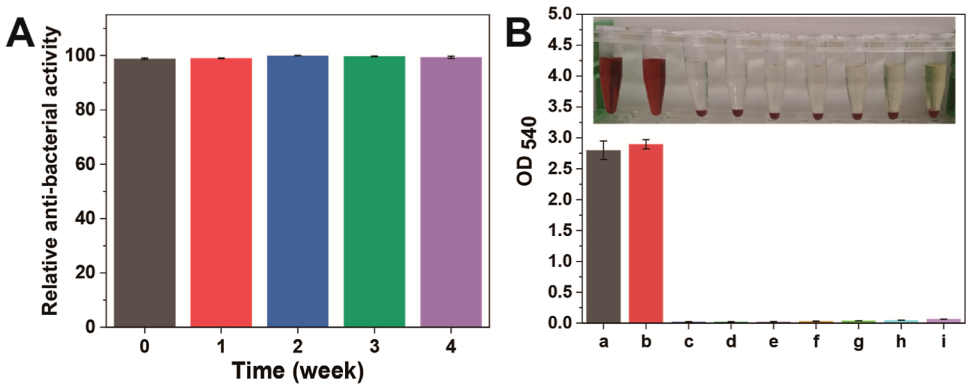

Figure 4. (A) Antibacterial stability of ATT-AuNCs. (B) Hemolytic activity of mouse blood after treatment with 0.1% triton, water, and various concentrations of ATT-AuNCs (a−i: 0.1% triton, water, 0, 8, 16, 32 64, 128, and 256 μg/mL).

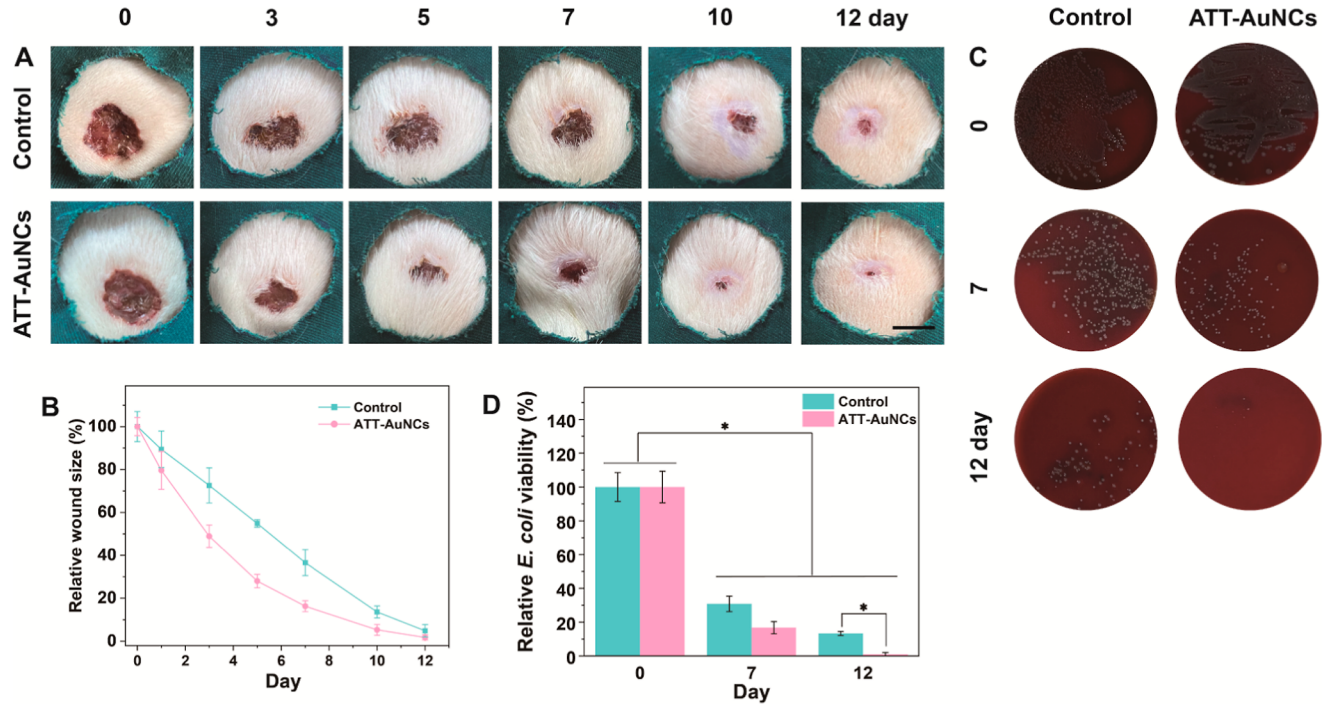

Figure 5. Therapeutic effect of ATT-AuNCs on a SD rat skin infection model. (A) Representative photographs of the healing processes of MDR *E. coli*-infected wounds (0, 3, 5, 7, 10, and 12 day). (B) The relative wound sizes (relative area vs starting area) at days 0, 1, 3, 5, 7, 10, and 12. (C) Bacteria colonies formation of MDR *E. coli* after different separation times (0, 7, and 12 day). (D) Quantitative analysis of MDR *E. coli* colonies from the infected wound at days 0, 7, and 12 (n = 3).

using RT-PCR analysis.[38] 4-oxalocrotonate tautomerase (encoded by dmpI gene) in the step of the oxidative catabolism is considered to be responsible for the oxidation of toluene, o-xylene, 3-ethyltoluene, and 1,2,4-trimethylbenzene, then converting into the citric acid cycle intermediates, followed by the generation of ROS as a byproduct.[39] Respiratory nitrate reductase (encoded by narJ and narK gene), and nitrate reductase (encoded by narK gene) can transfer electrons from NADH or NADPH to nitrate, and the nitrate transport coupled to nitrate reduction, respectively.[40] As shown in Figure 3F, we observed significantly higher expression levels of dmpI, narJ, and narK genes in the treatment group than that of the negative group. These results suggested that ATT-AuNC-activated upregulation of genes encoding the oxidative metabolic enzymes induced more pro-oxidative enzymes to be intracellularly expressed in MDR *E. coli* due to the impairment of bacterial cell walls.[17] The process of the preparation of ATT-AuNCs and the potential antimicrobial mechanism are shown in Scheme 1.

3.3. Antimicrobial Stability and Biocompatibility Evaluation. The long-term antimicrobial stability and hemolysis activity of ATT-AuNCs are significant and prerequisite performance indices for possible clinical applications. As shown in Figure 4A, ATT-AuNCs possessed good long-term antibacterial stability with 4 weeks. Moreover, Figure 4B shows hemolytic activity of ATT-AuNCs after 2 h incubation with fresh mouse blood. It was found that ATT-AuNCs have no hemolytic activity against erythrocytes at different tested concentrations. Our findings suggested the good biocompatibility of ATT-AuNCs.[27]

3.4. Promotion of Infected Wound Healing. We further evaluated the antimicrobial effect of ATT-AuNCs in SD rats infected with MDR *E. coli*. Figure 5A displayed photographs of wounds on rats from both groups at different times during the

https://doi.org/10.1021/acsomega.3c07114
ACS Omega 2023, 8, 47123−47133

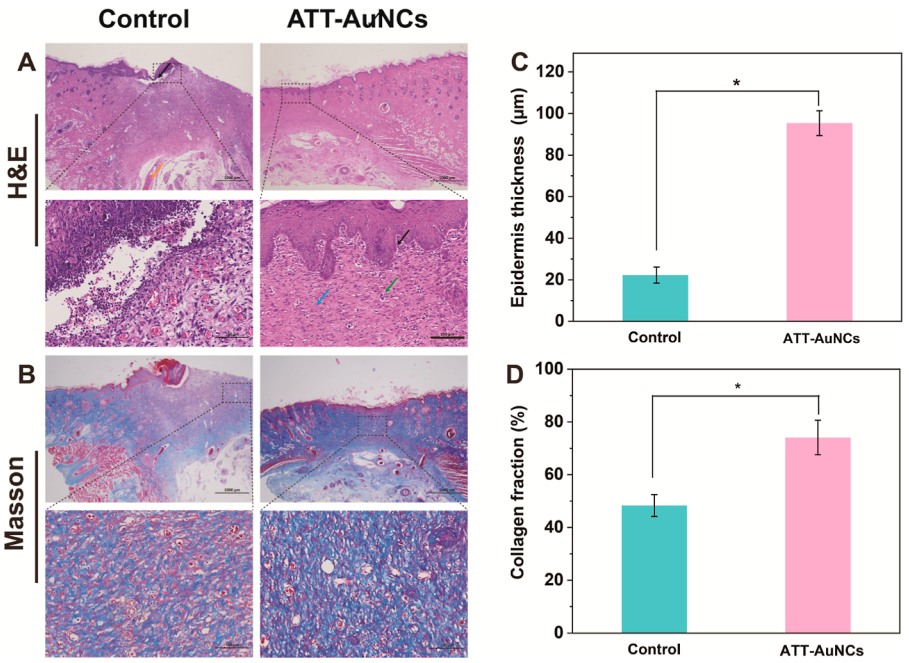

Figure 6. (A) H&E and (B) MT staining of wound sections in both groups on day 12. Scale bar: 100 μm. (C) Thickness of newly formed epidermis (n = 3). (D) Collagen accumulation on day 12 based on MT staining.

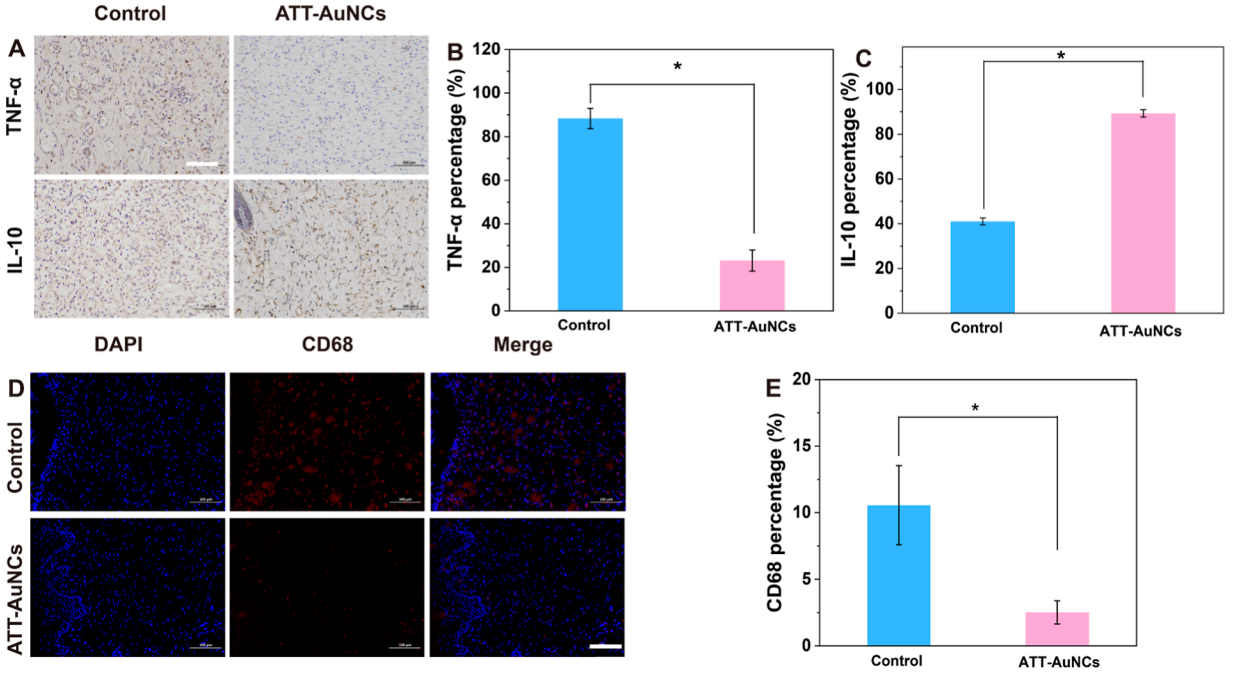

Figure 7. (A) Immunohistochemical staining of tumor necrosis factor (TNF)-α and IL-10 in the control and ATT-AuNCs groups. Quantification of the inflammatory area was based on TNF-α (B) and IL-10 (C) staining, respectively. Scale bar: 200 μm. (D) Immunofluorescence staining and (E) quantification percentage of CD68+ cells on day 12. Scale bar: 100 μm.

therapeutic process. After infection by MDR *E. coli* for 24 h, ulceration and suppuration were observed on both groups. After 3 days treatment, the wound site in the ATT-AuNCs group started to form a scab with a 52.1% reduction, while the water-treated group decreased only by 28.4%. On the 12th day, the water-treated wound area remained as high as 4.9%, which was only remained 1.8% in the ATT-AuNC-treated group (Figure 5B). Clearly, MDR *E. coli* infection and exudate can lead to prolonged wound healing.[41] In addition, the antibacterial properties of ATT-AuNCs were evaluated via seeding bacteria on blood agar plates from the wound sites. As displayed in Figure 5C, bacterial colonies from both groups obviously appeared on the agar. After 7 days of treatment, the density of bacteria from wounds treated with ATT-AuNCs was significantly reduced. However, on the 12th day, the wound of the control group produced drastically more bacterial colonies than the ATT-AuNC-treated group (Figure 5D). These results suggested that ATT-AuNCs have excellent antibacterial activity against infected wounds.

https://doi.org/10.1021/acsomega.3c07114
ACS Omega 2023, 8, 47123−47133

To further elevate the excellent wound-healing efficacy, hematoxy and eosin (H&E) and MT stained were employed for histological analysis. As shown in Figure 6A, more new blood vessels (green arrow) as well as the epidermis are gradually formed (black arrows), and a high collagen fiber surface area (blue arrow) appeared on the wound treated with ATT-AuNCs, while an incomplete epidermal layer (marked by black arrows) and a large number of inflammatory cells (orange arrows) emerged in the control group. The skin layer thickness of the fiber is further analyzed on day 12. As displayed in Figure 6C, the new epidermal layer was thicker in the ATT-AuNCs group (~95.3 μm) than in the control group (~21.5 μm), suggesting the acceleration of wound healing and restoration of the normal skin structure by treatment with ATT-AuNCs. Moreover, the Masson staining results are shown in Figure 6B, in which the wound area of the ATT-AuNC-treated group is more dense, revealing an extensive collagen deposition. As displayed in Figure 6D, the regenerated skin tissues treated with ATT-AuNCs present more collagen fibers (~74.1%) with deeper colors than the control group (~48.3%), confirming their contribution to the promotion of wound healing.[42] Additionally, Figure S2 shows that the main organs (heart, liver, spleen, lung, and kidney) of the rats had no significant difference between both groups, suggesting no adverse effect in rats.

Tumor necrosis factor (TNF)-α has been elucidated as a critical contributor in promotion of inflammatory diseases.[43] On the contrary, IL-10 is one of the stronger pleiotropic cytokines whose modulation triggers a cascade of signaling events involving anti-inflammatory activities.[44] Hence, an ideal antimicrobial wound therapy would include the inhibition of TNF-α and the promotion of IL-10 expression. As shown in Figure 7A, it could be found that more IL-10 positive staining was obviously observed in the wound tissue, which was treated by ATT-AuNCs, while less TNF-α positive staining was found in the wounds treated with ATT-AuNCs compared to the control group. Figure 7B,C also reveals that TNF-α, in the ATT-AuNC-treated group, reduced 65.2%, whereas IL-10 increased 48.2%, relative to the control group. CD68 is a biomarker of macrophages around the wound site, and excessive or prolonged inflammation can lead to delayed healing.[45] Figure 7D presents the results of CD68 immunofluorescence staining for macrophages in the wound sites of SD rats at day 12 after treatment. The ATT-AuNCs group has a smaller amount of CD68+ cells (~2.5%) than the control groups (~13.5%), revealing that the ATT-AuNCs could suppress the inflammation (Figure 7E). Overall, it was found that ATT-AuNCs show excellent antimicrobial and immunomodulatory properties in vivo while further promoting collagen deposition in the process of wound healing, increasing anti-inflammatory cytokine, and reducing wound irritation.

4. CONCLUSIONS

In this work, we have developed a kind of long-term stability and high-efficiency antibacterial ATT-AuNCs toward MDR *E. coli*. We suggest that negatively charged sulfur and oxygen functional groups serve to mask divalent cations (e.g., Ca^{2+}) on the surface of MDR *E. coli*, thereby enabling ATT-AuNCs to interact and perturb bacterial membranes. The generation of ROS induced by ATT-AuNCs could oxidize bacterial membrane and upregulate the expression of pro-oxidative relative genes. Furthermore, the effect of ATT-AuNCs was more dramatic through the leakage of protein and DNA damage, subsequently leading to a better bacterial killing efficiency. Additionally, the ATT-AuNCs have no detrimental effect on erythrocytes. Most importantly, the ATT-AuNCs exhibited a great anti-inflammatory property to promote wound healing in drug-resistant bacterial infected wounds in vivo. This study extends the versatility of AuNC-based materials, the emergence of ATT-AuNCs also provides a new approach for other biomedical applications such as cancer therapy.

■ ASSOCIATED CONTENT

Supporting Information

The Supporting Information is available free of charge at https://pubs.acs.org/doi/10.1021/acsomega.3c07114.

Materials and methods, apparatus and characterization, statistical analysis, characterization of ATT-AuNCs, detection of free radicals, and photomicrographs of the internal organs stained with H&E (PDF)

■ AUTHOR INFORMATION

Corresponding Authors

Ying-Ying Xu − *Department of Pharmaceutics, School of Pharmacy, Fujian Medical University, Fuzhou 350004, China*; Email: yingyingxu2017@fjmu.edu.cn

Wei Chen − *Fujian Key Laboratory of Drug Target Discovery and Structural and Functional Research, School of Pharmacy, Fujian Medical University, Fuzhou 350004, China*; orcid.org/0000-0003-3233-8877; Email: chenandhu@163.com

Quan-Quan Zhuang − *Department of Pharmacy, Affiliated Quanzhou First Hospital of Fujian Medical University, Quanzhou 362000, China*; Email: zhuangqq83@163.com

Authors

Hui-Qiong Jiang − *Department of Cardiac Function Examination Room, Affiliated Quanzhou First Hospital of Fujian Medical University, Quanzhou 362000, China*

Lin-Yan Lu − *Fujian Key Laboratory of Drug Target Discovery and Structural and Functional Research, School of Pharmacy, Fujian Medical University, Fuzhou 350004, China*

Zhi-Min Weng − *Fujian Key Laboratory of Drug Target Discovery and Structural and Functional Research, School of Pharmacy, Fujian Medical University, Fuzhou 350004, China*

Kai-Yuan Huang − *Fujian Key Laboratory of Drug Target Discovery and Structural and Functional Research, School of Pharmacy, Fujian Medical University, Fuzhou 350004, China*

Yu Yang − *Fujian Key Laboratory of Drug Target Discovery and Structural and Functional Research, School of Pharmacy, Fujian Medical University, Fuzhou 350004, China*

Hao-Hua Deng − *Fujian Key Laboratory of Drug Target Discovery and Structural and Functional Research, School of Pharmacy, Fujian Medical University, Fuzhou 350004, China*; orcid.org/0000-0002-3810-0686

Complete contact information is available at: https://pubs.acs.org/10.1021/acsomega.3c07114

Author Contributions

⊥H.-Q.J. and L.-Y.L. contributed equally to this work.

https://doi.org/10.1021/acsomega.3c07114
ACS Omega 2023, 8, 47123−47133

Notes

The authors declare no competing financial interest.

■ ACKNOWLEDGMENTS

The authors gratefully acknowledge financial support of the Program for Innovative Leading Talents in Fujian Province (2016B016), Program for Innovative Research Team in Science and Technology in Fujian Province University (2018B033), the National Natural Science Foundation of China (82204324), the Medical Elite Cultivation Program of Fujian (2020GGB049), the Science and Technology Project of Quanzhou (2022NS052), and Major Scientific Research Program for Young and Middle-aged Health Professionals of Fujian Province, China (2021ZQNZD015).

■ REFERENCES

(1) Abat, C.; Fournier, P. E.; Jimeno, M. T.; Rolain, J. M.; Raoult, D. Extremely and Pandrug-Resistant Bacteria Extra-Deaths: Myth or Reality? *Eur. J. Clin. Microbiol. Infect. Dis.* **2018**, *37*, 1687−1697.

(2) Nilsson, A. I.; Berg, O. G.; Aspevall, O.; Kahlmeter, G.; Andersson, D. I. Biological Costs and Mechanisms of Fosfomycin Resistance in Escherichia coli. *Antimicrob. Agents Chemother.* **2003**, *47*, 2850−2858.

(3) Webber, M. A.; Piddock, L. J. V. The importance of Efflux Pumps in Bacterial Antibiotic Resistance. *J. Antimicrob. Chemother.* **2003**, *51*, 9−11.

(4) Yuan, K.; Mei, Q.; Guo, X.; Xu, Y.; Yang, D.; Sánchez, B. J.; Sheng, B.; Liu, C.; Hu, Z.; Yu, G.; Ma, H.; Gao, H.; Haisch, C.; Niessner, R.; Jiang, Z.; Zhou, H. Antimicrobial Peptide Based Magnetic Recognition Elements and Au@Ag-GO SERS Tags with Stable Internal Standards: a Three in One Biosensor for Isolation, Discrimination and Killing of Multiple Bacteria in Whole Blood. *Chem. Sci.* **2018**, *9*, 8781−8795.

(5) Liu, L. H.; Xu, K. J.; Wang, H. Y.; Jeremy Tan, P. K.; Fan, W. M.; Venkatraman, S. S.; Li, L. J.; Yang, Y. Y. Self-Assembled Cationic Peptide Nanoparticles as an Efficient Antimicrobial Agent. *Nat. Nanotechnol.* **2009**, *4*, 457−463.

(6) Shi, L. W.; Zhuang, Q. Q.; Wang, T. Q.; Jiang, X. D.; Liu, Y.; Deng, J. W.; Sun, H. H.; Li, Y.; Li, H. H.; Liu, T. B.; Liu, J. Z. Synthetic Antibacterial Quaternary Phosphorus Salts Promote Methicillin-Resistant *Staphylococcus aureus*-Infected Wound Healing. *Int. J. Nanomed.* **2023**, *18*, 1145−1158.

(7) Shen, C.; Xue, Y.; Li, Y.; Wei, M.; Wen, M.; Zhang, L.; Shang, L. Kinetically Regulated One-Pot Synthesis of Cationic Gold Nanoparticles and Their Size-Dependent Antibacterial Mechanism. *J. Mater. Sci. Technol.* **2023**, *162*, 145−156.

(8) Haidari, H.; Kopecki, Z.; Bright, R.; Cowin, A. J.; Garg, S.; Goswami, N.; Vasilev, K. Ultrasmall AgNP-Impregnated Biocompatible Hydrogel with Highly Effective Biofilm Elimination Properties. *ACS Appl. Mater. Interfaces* **2020**, *12*, 41011−41025.

(9) Awasthi, A.; Sharma, P.; Jangir, L.; Kamakshi; Awasthi, G.; Awasthi, K. K.; Awasthi, K. Dose Dependent Enhanced Antibacterial Effects and Reduced Biofilm Activity Against Bacillus Subtilis in Presence of ZnO Nanoparticles. *Mater. Sci. Eng., C* **2020**, *113*, 111021.

(10) Nie, L.; Chang, P. B.; Ji, C. C.; Zhang, F.; Zhou, Q. J.; Sun, M.; Sun, Y.; Politis, C.; Shavandi, A. Poly(acrylic acid) capped iron oxide nanoparticles via ligand exchange with antibacterial properties for biofilm applications. *Colloids Surf., B* **2021**, *197*, 111385.

(11) Abdulsada, F. M.; Hussein, N. N.; Sulaiman, G. M.; Al Ali, A.; Alhujaily, M. Evaluation of the Antibacterial Properties of Iron Oxide, Polyethylene Glycol, and Gentamicin Conjugated Nanoparticles Against Some Multidrug-Resistant Bacteria. *J. Funct. Biomater.* **2022**, *13*, 138.

(12) Du, J.; Wang, S.; Luo, P.; Han, X.; Bai, X.; Zhu, E.; Liu, C.; Guo, H.; Ma, C. Nature Sunlight-Driven Polymer/TiO_2 Antimicrobial Agent for the Killing of Multidrug-Resistant Bacteria with Enhanced Photocatalytic Activity. *J. Photochem. Photobiol., A* **2023**, *444*, 114973.

(13) Vimbela, G. V.; Ngo, S. M.; Fraze, C.; Yang, L.; Stout, D. A. Antibacterial properties and toxicity from metallic nanomaterials. *Int. J. Nanomed.* **2017**, *12*, 3941−3965.

(14) Yang, J.; Peng, Y.; Li, S.; Mu, J.; Huang, Z.; Ma, J.; Shi, Z.; Jia, Q. Metal nanocluster-based hybrid nanomaterials: Fabrication and application. *Chem. Rev.* **2022**, *456*, 214391.

(15) Kuo, J. C.; Tan, S. H.; Hsiao, Y. C.; Mutalik, C.; Chen, H. M.; Yougbaré, S.; Kuo, T. R. Unveiling the Antibacterial Mechanism of Gold Nanoclusters via in Situ Transmission Electron Microscopy. *ACS Sustainable Chem. Eng.* **2022**, *10*, 464−471.

(16) Xie, Y.; Liu, Y.; Yang, J.; Liu, Y.; Hu, F.; Zhu, K.; Jiang, X. Gold Nanoclusters for Targeting Methicillin-Resistant *Staphylococcus aureus* In Vivo. *Angew. Chem., Int. Ed.* **2018**, *57*, 3958−3962.

(17) Zheng, K.; Setyawati, M. I.; Leong, D. T.; Xie, J. Observing Antimicrobial Process with Traceable Gold Nanoclusters. *Nano Res.* **2021**, *14*, 1026−1033.

(18) Zheng, Y.; Liu, W.; Qin, Z.; Chen, Y.; Jiang, H.; Wang, X. Mercaptopyrimidine-Conjugated Gold Nanoclusters as Nanoantibiotics for Combating Multidrug-Resistant Superbugs. *Bioconjugate Chem.* **2018**, *29*, 3094−3103.

(19) Li, Y.; Zhen, J.; Tian, Q.; Shen, C.; Zhang, L.; Yang, K.; Shang, L. One Step Synthesis of Positively Charged Gold Nanoclusters as Effective Antimicrobial Nanoagents Against Multidrug-Resistant Bacteria and Biofilms. *J. Colloid Interface Sci.* **2020**, *569*, 235−243.

(20) Chang, T. K.; Cheng, T. M.; Chu, H. L.; Tan, S. H.; Kuo, J. C.; Hsu, P. H.; Su, C. Y.; Chen, H. M.; Lee, C. M.; Kuo, T. R. Metabolic Mechanism Investigation of Antibacterial Active CysteineConjugated Gold Nanoclusters in Escherichia coli. *ACS Sustainable Chem. Eng.* **2019**, *7*, 15479−15486.

(21) Deng, H. H.; Shi, X. Q.; Peng, H. P.; Zhuang, Q. Q.; Yang, Y.; Liu, A. L.; Xia, X. H.; Chen, W. Gold Nanoparticle-Based Photoluminescent Nanoswitch Controlled by Host-Guest Recognition and Enzymatic Hydrolysis for Arginase Activity Assay. *ACS Appl. Mater. Interfaces* **2018**, *10*, 5358−5364.

(22) Ran, X.; Du, Y.; Wang, Z. Z.; Wang, H.; Pu, F.; Ren, J. S.; Qu, X. G. Hyaluronic Acidtemplated Ag Nanoparticles/Graphene Oxide Composites for Synergistic Therapy of Bacteria Infection. *ACS Appl. Mater. Interfaces* **2017**, *9*, 19717−19724.

(23) Zhu, Z.; Bai, Q.; Li, S.; Li, S.; Liu, M.; Du, F.; Sui, N.; Yu, W. W. Antibacterial Activity of Graphdiyne and Graphdiyne Oxide. *Small* **2020**, *16*, 2001440.

(24) Xiong, J.; Cao, Y.; Zhao, H.; Chen, J.; Cai, X.; Li, X.; Liu, Y.; Xiao, H.; Ge, J. Cooperative Antibacterial Enzyme-AgPolymer Nanocomposites. *ACS Nano* **2022**, *16*, 19013−19024.

(25) Zhang, T.; Deng, Y.; Liu, Y. S.; Chua, S. L.; Tang, B. Z.; Khoo, B. L. Bacterial Targeted AIE Photosensitizers Synergistically Promote Chemotherapy for the Treatment of Inflammatory Cancer. *Chem. Eng. J.* **2022**, *447*, 137579.

(26) Zheng, K.; Setyawati, M. I.; Leong, D. T.; Xie, J. Surface Ligand Chemistry of Gold Nanoclusters Determines Their Antimicrobial Ability. *Chem. Mater.* **2018**, *30*, 2800−2808.

(27) Xie, Y.; Zhang, Q.; Zheng, W.; Jiang, X. Small Molecule-Capped Gold Nanoclusters for Curing Skin Infections. *ACS Appl. Mater. Interfaces* **2021**, *13*, 35306−35314.

(28) Deng, H. H.; Shi, X. Q.; Wang, F. F.; Peng, H. P.; Liu, A. L.; Xia, X. H.; Chen, W. Fabrication of Water-Soluble, Green-Emitting Gold Nanoclusters with a 65% Photoluminescence Quantum Yield via Host-Guest Recognition. *Chem. Mater.* **2017**, *29*, 1362−1369.

(29) Deng, H. H.; Huang, K. Y.; Zhuang, Q. Q.; Zhuang, Q. Q.; Peng, H. P.; Liu, Y. H.; Xia, X. H.; Chen, W. Preparation of Strongly Fluorescent Water-Soluble Dithiothreitol Modified Gold Nanoclusters Coated with Carboxychitosan, and Their Application to Fluorometric Determination of the Immunosuppressive 6-Mercaptopurine. *Microchim. Acta* **2018**, *185*, 400.

(30) Shang, L.; Azadfar, N.; Stockmar, F.; Send, W.; Trouillet, V.; Bruns, M.; Gerthsen, D.; Nienhaus, G. U. One-Pot Synthesis of

https://doi.org/10.1021/acsomega.3c07114
ACS Omega 2023, 8, 47123−47133

Nearinfrared Fluorescent Gold Clusters for Cellular Fluorescence Lifetime Imaging. *Small* **2011**, *7*, 2614−2620.
(31) Baek, S.; Joo, S. H.; Su, C.; Toborek, M. Antibacterial Effects of Graphene- and Carbon-Nanotube-Based Nanohybrids on Escherichia coli: Implications for Treating Multidrug-Resistant Bacteria. *J. Environ. Manage.* **2019**, *247*, 214−223.
(32) Zhu, C.; Yang, Q.; Liu, L.; Lv, F.; Li, S.; Yang, G.; Wang, S. Multifunctional Cationic Poly(p-phenylene vinylene) Polyelectrolytes for Selective Recognition, Imaging, and Killing of Bacteria Over Mammalian Cells. *Adv. Mater.* **2011**, *23*, 4805−4810.
(33) Tong, C.; Zhong, X.; Yang, Y.; Liu, X.; Zhong, G.; Xiao, C.; Liu, B.; Wang, W.; Yang, X. PB@PDA@Ag Nanosystem for Synergistically Eradicating MRSA and Accelerating Diabetic Wound Healing Assisted with Laser Irradiation. *Biomaterials* **2020**, *243*, 119936.
(34) Zhao, R.; Kong, W.; Sun, M.; Yang, Y.; Liu, W.; Lv, M.; Song, S.; Wang, L.; Song, H.; Hao, R. Highly Stable Graphene-Based Nanocomposite (GO-PEI-Ag) with Broad-Spectrum, Long-Term Antimicrobial Activity and Antibiofilm Effects. *ACS Appl. Mater. Interfaces* **2018**, *10*, 17617−17629.
(35) Michiels, J.; Xi, C.; Verhaert, J.; Vanderleyden, J. The Functions of Ca^{2+} in Bacteria: a Role for EF-Hand Proteins? *Trends Microbiol.* **2002**, *10*, 87−93.
(36) Ho, S. W.; Jung, D.; Calhoun, J. R.; Lear, J. D.; Okon, M.; Scott, W. R. P.; Hancock, R. E. W.; Straus, S. K. Effect of Divalent Cations on the Structure of the Antibiotic Daptomycin. *Eur. Biophys. J.* **2008**, *37*, 421−433.
(37) Le Guével, X.; Hotzer, B.; Jung, G.; Hollemeyer, K.; Trouillet, V.; Schneider, M. Formation of Fluorescent Metal (Au, Ag) Nanoclusters Capped in Bovine Serum Albumin Followed by Fluorescence and Spectroscopy. *J. Phys. Chem. C* **2011**, *115*, 10955−10963.
(38) Ben-Ami, R.; Klochendler, A.; Seidel, M.; Sido, T.; Gurel-Gurevich, O.; Yassour, M.; Meshorer, E.; Benedek, G.; Fogel, I.; Oiknine-Djian, E.; Gertler, A.; Rotstein, Z.; Lavi, B.; Dor, Y.; Wolf, D. G.; Salton, M.; Drier, Y.; et al. Large-Scale Implementation of Pooled RNA Extraction and RT-PCR for SARS-CoV-2 Detection. *Clin. Microbiol. Infect.* **2020**, *26*, 1248−1253.
(39) Whitman, C. P. The 4-Oxalocrotonate Tautomerase Family of Enzymes: How Nature Makes New Enzymes Using a β-α-β Structural Motif. *Arch. Biochem. Biophys.* **2002**, *402*, 1−13.
(40) Fuchs, S.; Pané-Farré, J.; Kohler, C.; Hecker, M.; Engelmann, S. Anaerobic Gene Expression in *Staphylococcus aureus*. *J. Bacteriol.* **2007**, *189*, 4275−4289.
(41) Lu, B.; Lu, F.; Ran, L.; Yu, K.; Xiao, Y.; Li, Z.; Dai, F.; Wu, D.; Lan, G. Self-Assembly of Natural Protein and Imidazole Molecules on Gold Nanoparticles: Applications in Wound Healing Against Multi-Drug Resistant Bacteria. *Int. J. Biol. Macromol.* **2018**, *119*, 505−516.
(42) Wang, Y.; Zhao, Y.; Wu, J.; Li, M.; Tan, J.; Fu, W.; Tang, H.; Zhang, P. Negatively Charged Sulfur Quantum Dots for Treatment of DrugResistant Pathogenic Bacterial Infections. *Nano Lett.* **2021**, *21*, 9433−9441.
(43) Coll, R. C.; Robertson, A. A.; Chae, J. J.; Higgins, S. C.; MunozPlanillo, R.; Inserra, M. C.; Vetter, I.; Dungan, L. S.; Monks, B. G.; Stutz, A.; Croker, D. E.; Butler, M. S.; Haneklaus, M.; Sutton, C. E.; Nunez, G.; Latz, E.; Kastner, D. L.; Mills, K. H.; Masters, S. L.; Schroder, K.; Cooper, M. A.; O'Neill, L. A. A Small-Molecule Inhibitor of the NLRP3 Inflammasome for the Treatment of Inflammatory Diseases. *Nat. Med.* **2015**, *21*, 248−255.
(44) Kamaly, N.; Fredman, G.; Fojas, J. J.; Subramanian, M.; Choi, W. I.; Zepeda, K.; Vilos, C.; Yu, M.; Gadde, S.; Wu, J.; Milton, J.; Carvalho Leitao, R.; Rosa Fernandes, L.; Hasan, M.; Gao, H.; Nguyen, V.; Harris, J.; Tabas, I.; Farokhzad, O. C. Targeted Interleukin-10 Nanotherapeutics Developed with a Microfluidic Chip Enhance Resolution of Inflammation in Advanced Atherosclerosis. *ACS Nano* **2016**, *10*, 5280−5292.
(45) Qin, J.; Li, M.; Yuan, M.; Shi, X.; Song, J.; He, Y.; Mao, H.; Kong, D.; Gu, Z. Gallium(III)-Mediated Dual-Cross-Linked Alginate Hydrogels with Antibacterial Properties for Promoting Infected Wound Healing. *ACS Appl. Mater. Interfaces* **2022**, *14*, 22426−22442.

https://doi.org/10.1021/acsomega.3c07114
ACS Omega 2023, 8, 47123−47133